Acta Crystallographica Section D
Biological Crystallography
ISSN 0907-4449

The structure of *Vibrio cholerae* extracellular endonuclease I reveals the presence of a buried chloride ion

Bjørn Altermark,[a] Arne O. Smalås,[a] Nils P. Willassen[a,b] and Ronny Helland[a]*

[a]The Norwegian Structural Biology Centre, Faculty of Science, University of Tromsø, N-9037 Tromsø, Norway, and [b]Department of Molecular Biotechnology, Faculty of Medicine, University of Tromsø, N-9037 Tromsø, Norway

Correspondence e-mail: ronny.helland@chem.uit.no

Received 8 March 2006
Accepted 25 August 2006

PDB References: *Vc*EndA, low-pH form, 2g7e, r2g7esf; neutral-pH form, 2g7f, r2g7fsf.

The crystal structure of a periplasmic/extracellular endonuclease from *Vibrio cholerae* has been solved at low and at neutral pH. Crystals grown at pH 4.6 and 6.9 diffracted to 1.6 Å (on BM01A at the ESRF) and 1.95 Å (on a rotating-anode generator), respectively. The structures of the endonuclease were compared with the structure of a homologous enzyme in *V. vulnificus*. The structures of the *V. cholerae* enzyme at different pH values are essentially identical to each other and to the *V. vulnificus* enzyme. However, interesting features were observed in the solvent structures. Both *V. cholerae* structures reveal the presence of a chloride ion completely buried within the core of the protein, with the nearest solvent molecule approximately 7 Å away. Magnesium, which is essential for catalysis, is present in the structure at neutral pH, but is absent at low pH, and may partly explain the inactivity of the enzyme at lower pH.

1. Introduction

Vibrio cholerae possesses two extracellular nucleases of approximately 100 and 25 kDa (Focareta & Manning, 1991*a*). The smaller nuclease, here called *Vc*EndA, has been shown to be the major extracellular nuclease of this bacterium, accounting for most of the extracellular nuclease activity. The exact function of the nuclease is not yet known, but it probably provides nucleic acids for the cell. The nuclease is not believed to be involved in the pathogenicity of the bacterium (Focareta & Manning, 1991*a*), but it has been suggested that the nuclease can help the pathogen through the mucus layers of the host by degrading the nucleic acids in the mucus and hence decreasing the mucus viscosity. The difficulties observed when trying to transform the bacterium with plasmids also arise from this nuclease. The lower transformation efficiency caused by the nuclease implies a protective function against invading DNA (Focareta & Manning, 1991*a*). The crystal structure of *V. vulnificus* endonuclease I (Vvn) has been solved in both the native form and as an active-site mutant in complex with DNA (PDB codes 1ouo and 1oup, respectively; Li *et al.*, 2003). The catalytic mechanism proposed by the authors suggests that His80 functions as the general base, which activates a water molecule for an in-line attack on the scissile phosphate. The role of the magnesium ion is to stabilize the phosphoanion transition state and to make a proton available for the 3′-oxygen leaving group *via* a bound water molecule. Arg99 is thought to stabilize the product *via* a hydrogen bond to the phosphate, which also decelerates the reverse reaction. Vvn is located in the periplasmic space of the bacterium (Wu *et al.*, 2001), in contrast to *Vc*EndA which is exported extracellularly (Focareta & Manning, 1991*b*). In *Escherichia coli*, the recom-

Table 1
Data-collection and refinement statistics.

Values for the outer shell (1.69–1.60 and 2.06–1.95 Å for the low-pH and neutral-pH forms, respectively) are indicated in parentheses.

	pH 4.6	pH 6.9
Data collection		
Diffraction limit	1.60	1.95
Unit-cell parameters (Å)	a = 40.52, b = 64.16, c = 75.57	a = 40.40, b = 64.75, c = 75.78
Space group	$P2_12_12_1$	$P2_12_12_1$
Wavelength (Å)	0.8737 (BM01A, ESRF)	1.54180 (rotating anode)
Total No. of reflections	121474 (17566)	41893 (2045)
No. of unique reflections	26728 (3846)	13324 (1019)
Completeness (%)	100 (100)	88.8 (49.0)†
Anomalous completeness		80.0 (28.7)‡
$I/\sigma(I)$	9.1 (1.9)	9.2 (2.0)
$R_{\rm merge}$ (%)	5.5 (38.9)	7.5 (37.8)
Multiplicity	4.5 (4.6)	3.1 (2.0)
Wilson B factor (Å^2)	16.34	18.03
Refinement		
$R_{\rm work}$ (%)	22.25	17.67
$R_{\rm free}$ (%)	25.52	23.31
Average B factors (Å^2)	17.68	14.23
No. protein atoms	1660	1654
No. solvent molecules (including Mg^{2+} and Cl^-)	164	179
R.m.s. deviations		
Bond lengths (Å)	0.013	0.017
Bond angles (°)	1.487	1.446
Ramachandran plot, residues in (%)		
Most favoured regions	93.4	95.1
Additionally allowed regions	5.5	3.8
Generously allowed regions	1.1	1.1
Disallowed regions	0	0

† Cumulative completeness is 95% to 2.06 Å. ‡ Anomalous completeness is 96.6% to 2.2 Å (91.0% for the 2.3–2.2 Å resolution shell).

binant *Vc*EndA is shown to be periplasmic (Focareta & Manning, 1987). It is therefore proposed that *V. cholerae* possesses some kind of export machinery that is lacking in both *V. vulnificus* and *E. coli* (Focareta & Manning, 1991*b*).

Here, we present the structure of *V. cholerae* ATCC 14035 endonuclease I and compare its structural properties with those of *V. vulnificus* endonuclease I.

2. Materials and methods

2.1. Recombinant expression and purification

*Vc*EndA (GenBank accession No. DQ263605) was cloned, recombinantly expressed in *E. coli* and purified as described in Altermark (2006). Briefly, the periplasmic fraction from the harvested cells was applied onto an SP Sepharose column and eluted with a linear gradient of NaCl from 0 to 1 *M*. The purity of the concentrated enzyme was evaluated by SDS–PAGE.

2.2. Crystallization

Initial screening of crystallization conditions was conducted using Crystal Screen and Crystal Screen 2 from Hampton Research. Crystals of *Vc*EndA were obtained using the hanging-drop vapour-diffusion technique at room temperature. All drops were generated by mixing 2.0 µl enzyme solution (4.2 mg ml^{-1} in 20 m*M* Tris buffer pH 8.3, 10 m*M* $MgSO_4$ and approximately 0.6 *M* NaCl) with 2.0 µl precipitant solution and were equilibrated against 1.0 ml precipitant solution.

2.3. Data collection, structure determination and refinement

Crystals were soaked in precipitant solution containing 10% glycerol prior to flash-cooling in liquid nitrogen. X-ray intensity data were collected from a single low-pH crystal of approximate dimensions 0.3 × 0.08 × 0.08 mm on the Swiss–Norwegian Beamlines (SNBL, BM01A) at the European Synchrotron Radiation Facility (ESRF), Grenoble, France. X-ray data from a single neutral-pH crystal were collected using a Rigaku rotating-anode generator equipped with an R-AXIS IV image-plate detector system. Data from both crystals were processed using the programs *MOSFLM* (Powell, 1999), *SCALA* and *TRUNCATE* from the *CCP*4 program suite (Collaborative Computational Project, Number 4, 1994).

The low-pH structure was solved by molecular replacement using the program *MOLREP* (Vagin & Teplyakov, 1997) from *CCP*4, using the substrate-free structure of *V. vulnificus* endonuclease I (PDB code 1ouo) as a search model. The structure of the neutral-pH form was then determined using the refined low-pH structure as a starting model. The structures were built using a combination of autobuilding in *ARP*/*wARP* (Perrakis *et al.*, 1999) and manual refitting of side chains using *O* (Jones *et al.*, 1991) based on σ_A-weighted $2mF_o - DF_c$ and $mF_o - DF_c$ electron-density maps. Refinement was carried out in *REFMAC*5 (Murshudov *et al.*, 1997) from the *CCP*4 suite. The models were validated using *PROCHECK* (Laskowski *et al.*, 1993) and *WHATCHECK* (Hooft *et al.*, 1996).

The residue numbering of the catalytic domain of the *Vc*EndA structures follows that of the Vvn structure, starting at 20. This corresponds to residue 21 of the native *Vc*EndA sequence deposited in GenBank. In the structural comparison between Vvn and *Vc*EndA, the two forms of the latter are considered to be identical.

3. Results and discussion

3.1. Crystallization, data collection, structure determination and refinement

Optimization of the crystallization conditions found in the initial screens yielded diffraction-quality crystals of approximate dimensions of up to 0.3 × 0.08 × 0.08 mm from 25% PEG 4000, 0.1 *M* sodium acetate pH 4.6 and 0.3 *M* ammonium acetate (low-pH form) and 30% PEG 8000, 0.2 *M* sodium acetate and 0.1 *M* cacodylate buffer pH 6.9 (neutral-pH form).

The low-pH form diffracted to 1.6 Å, while the neutral-pH form diffracted to 1.95 Å. Data-collection and refinement characteristics are listed in Table 1. Both crystals belonged to space group $P2_12_12_1$, with similar unit-cell parameters of

approximately $a = 40$, $b = 64$, $c = 75$ Å and one molecule in the asymmetric unit.

MOLREP found one clear rotation solution for the low-pH form with a rotation function/σ value of 7.94, 3.5σ higher than the second best solution. Parts of the structure were poorly defined in electron density in the initial maps. These were therefore rebuilt by autobuilding using *ARP*/*wARP* in combination with manual refitting of side chains and loops. The structure of the neutral-pH form was determined by *MOLREP* using the refined low-pH structure as a starting model. One clear solution was found with a rotation function/σ value of 10.67.

The data for the low-pH structure are more complete and the scaling statistics are better than for the neutral-pH structure. Despite this, the electron density is comparable in the two structures and the *R* factors are slightly better for the data collected using the rotating-anode source ($R_{\rm work}$ and $R_{\rm free}$ of 17.67 and 23.31%, respectively, for the neutral-pH structure, and 22.25 and 25.52%, respectively, for the low-pH structure). The electron density is in general well defined for both structures, except at the N-termini where the first few residues are not defined at all in any of the structures. Parts of the N-terminus are involved in DNA binding in the Vvn structure (PDB code 1oup; Li *et al.*, 2003). Other regions with poorly defined side chains include residues belonging to or close to the DNA-binding sites, *i.e.* residues 68, 100 and 156. Residue 99, which is thought to stabilize the product after catalysis, is refined in two conformations in the low-pH structure. Other residues with poorly defined electron density are in or close to two epitopes involved in contacts with symmetry-related molecules. The majority of these residues are basic in both epitopes, thus creating an aggregation of positive potential that cannot be efficiently stabilized by negatively charged residues or solvent molecules.

3.2. General description of the structure

The main-chain atoms of the two structures superimpose on each other with an r.m.s.d. (root-mean-square deviation) of 0.18 Å, which is of the same order as the mean coordinate error of the structures. Including side chains, the two structures superimpose with an r.m.s.d. value of 0.52 Å, indicating that the structures, as expected, are practically identical. However, two interesting features were observed in the solvent structure of *Vc*EndA. The first was that no magnesium could be identified in the low-pH form of *Vc*EndA (Fig. 1*a*). This was not totally surprising, since the magnesium ion should be coordinated to the side chains of Glu79 $O^{\varepsilon1}$ and Asn127 $O^{\delta1}$ and four solvent molecules according to the Vvn structure. The theoretical pK_a for Glu is about 4.3, but it may vary in the microenvironment on the protein surface. At low pH, Glu79 is likely to be shifted towards the protonated state and hence the affinity for a magnesium ion will be reduced. We wanted, however, to verify that magnesium would actually be present at a pH where the enzyme is active and this is the reason why the structure was also solved at neutral pH. Electron density was found in the neutral-pH structure at the position equivalent to the magnesium position in Vvn with coordination geometry, distances to the coordinating O atoms (2.00–2.32 Å) and difference electron-density maps which all suggested a magnesium ion (Fig. 1*b*). The lack of magnesium in the low-pH structure does not seem to affect the enzyme or solvent structure significantly, because three of the solvent molecules found in the structure at neutral pH are present also in the magnesium-free structure at more or less identical positions. The orientation of the side chains of the residues surrounding the magnesium-binding site are also identical, with the exception of Arg99, which is, as mentioned above, refined with two conformations in the low-pH structure. Both orientations deviate slightly from the posi-

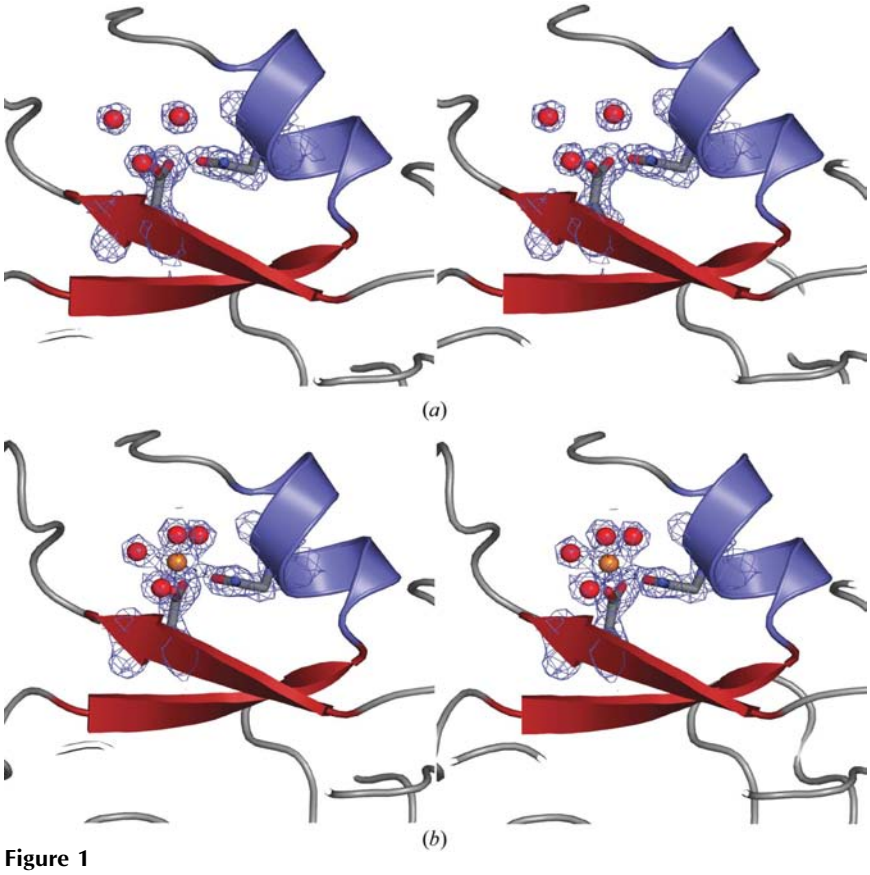

Figure 1
(*a*) Stereo plot illustrating the $2mF_o - DF_c$ electron-density map (contoured at 1.2σ) of the magnesium-free binding site in the *Vc*EndA structure at low pH. Glu79, Asn127 and three solvent molecules are displayed in ball-and-stick representation. (*b*) Stereo plot illustrating the $2mF_o - DF_c$ electron-density map (contoured at 1.5σ) of the magnesium-binding site in the *Vc*EndA structure at neutral pH. Glu79, Asn127, four solvent molecules and magnesium (orange) are displayed in ball-and-stick representation. This figure was prepared with *PyMOL* (DeLano, 2002).

tion of Arg99 in the structures with magnesium (*Vc*EndA and Vvn). Arg99 is located about 7 Å away from the magnesium ion. The activity of the enzyme is almost completely absent at pH below 6. The lack of magnesium in the low-pH structure therefore provides an explanation of the reduced activity of the enzyme at lower pH and it confirms the role and importance of the ion in the catalytic process (Li *et al.*, 2003).

The second feature observed in the *Vc*EndA structures (both at low and neutral pH) was extra difference electron density for a single solvent molecule in the interior of the enzyme, about 7 Å from the nearest solvent molecule and about 10 Å from the position where the magnesium ion was found. This molecule was interpreted as a chloride ion based on anomalous difference maps and electron density during refinement. The anomalous pairs had been kept separate in the data collected with copper radiation. Halides (Cl, Br and I) have anomalous signals at 1.54 Å (Cu radiation). The strength of the anomalous signal of chloride should be comparable to that of sulfur (theoretical f'' of about 0.7 and 0.6 e, respectively; http://skuld.bmsc.washington.edu/scatter/) and this is what is seen in Fig. 2(*a*). Both bromide and iodine have significantly stronger signals than chloride (about 1.3 and 6.9 e, respectively) and fluoride has no significant anomalous signal at this wavelength. The electron density does not match that of bromide, but matches perfectly with a chloride ion. The *B* factor of the refined chloride is also of the same order as the surrounding atoms. The chloride ion is 7.1 Å away from the nearest solvent molecule. It coordinates to three backbone N atoms in the interior of the structure (Tyr43, Cys44, Ile123) and O^{γ} of the buried Ser41. The distances range from about 3.0 to 3.5 Å and this corresponds to the chloride–nitrogen and chloride–oxygen distances reported for organic molecules (Steiner, 1998). Investigation of the same position in the Vvn structure identified a water molecule with a *B* factor of 1.17 $Å^2$. This indicates that a chloride could also be present there. The chloride-coordinating backbone N atoms belong to amino acids that are highly conserved among the homologous sequences investigated by Altermark (2006). The exact role of the chloride is not yet clear, but we believe that it is essential for the function and stability of the enzyme and that it is incorporated into the molecule during the folding process since there are no obvious diffusion channels. The chloride is surrounded by two of the four disulfide bridges found in *Vc*EndA (Cys44–Cys149 and Cys46–Cys62). Movement of side chains or loops in order to accommodate the insertion of the ion after the enzyme has been folded therefore seems to be severely restricted. Insertion of chloride after the protein is folded cannot, however, be completely ruled out.

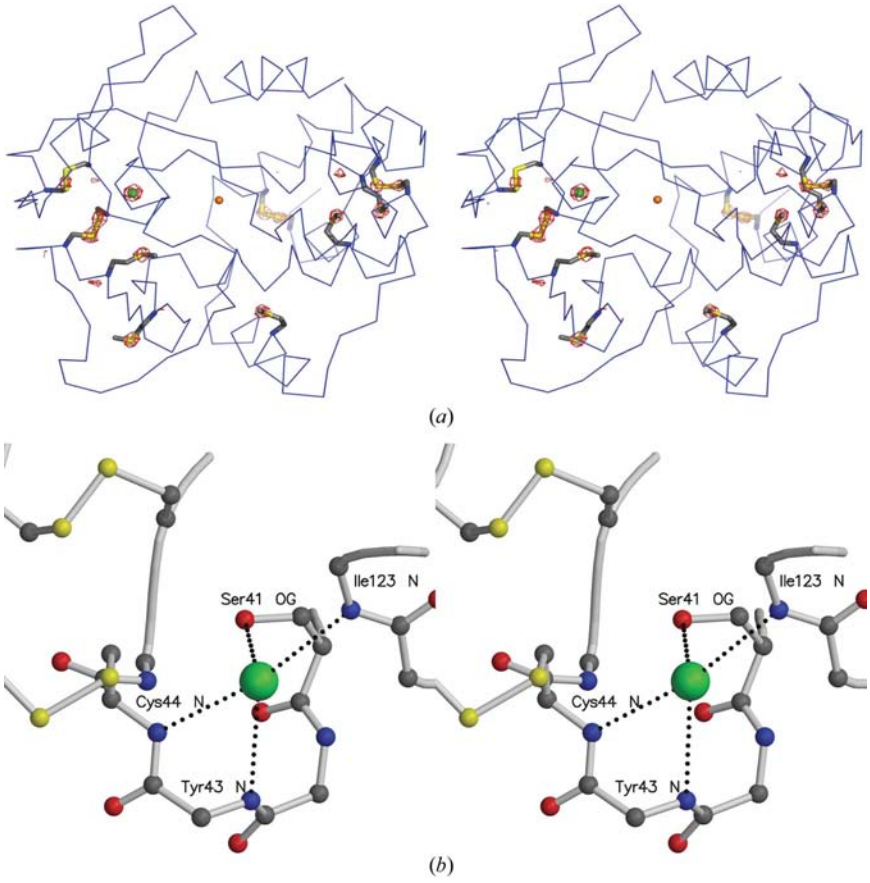

Figure 2
(*a*) Stereo plot illustrating the anomalous difference map (red) contoured at 4.5σ surrounding the buried chloride (green) in the interior of the protein and the S atoms (yellow). Magnesium is displayed as an orange sphere. (*b*) Stereo plot of the interactions between the chloride ion (green sphere) and the protein main-chain N atoms of Tyr43, Cys44, Ile123 and the O^{γ} atom of Ser41. Two disulfide bridges in the vicinity of the chloride-binding site are also displayed. This figure was prepared with *PyMOL* (DeLano, 2002) and *MOLSCRIPT* (Kraulis, 1991).

Searching the Macromolecular Structure Database (http://www.ebi.ac.uk/msd-srv/msdsite/statistics; Golovin *et al.*, 2005) for buried chloride ligands yielded a hit for only one other protein; the hormone-binding domain of the atrial natriuretic peptide (ANP) receptor (van den Akker *et al.*, 2000; He *et al.*, 2001; Ogawa *et al.*, 2004). The chloride in these structures is, as in *Vc*EndA, about 7 Å from the nearest solvent molecule and is next to a disulfide bridge. The chloride is expected to be an integral part of the protein because its surroundings do not change upon hormone binding (He *et al.*, 2001). The exact function of the chloride is not quite clear, but is expected to be important since depletion of chloride from the assay medium results in loss of ANP binding (van den Akker *et al.*, 2000). There is no structural similarity of the overall fold of the chloride-binding sites in *Vc*EndA and the ANP receptor, but the chloride in both proteins, in addition to being next to a disulfide bridge, form hydrogen bonds to the backbone N atoms of two adjacent residues and the hydroxyl group of a serine. The second of the backbone N atoms belongs to a Cys residue forming a disulfide bridge in both proteins.

3.3. Structural comparison to Vvn

The sequence identity between Vvn and *Vc*EndA is 73% and the main-chain atoms of *Vc*EndA superimpose on the substrate-free Vvn with r.m.s.d. values of 0.65 and 0.66 Å (low-pH and neutral-pH structures, respectively). Several of the regions that deviate more than the mean r.m.s.d. are close to regions involved in contact with symmetry-related molecules in one of the structures: 95–98 in Vvn, 216–218 in both structures and 37–38, 59–63, 66–67, 88–92, 103–110, 138–145 and 182–187 in *Vc*EndA. The orientation of the amino acids forming regions involved in ion binding (magnesium and chloride) is essentially identical in the enzymes from the two species. The amino-acid sequence of the regions forming the DNA-binding site is conserved, with the exception of residues 69 and 129 (Gln and Asp in Vvn, and Asn and Asn in *Vc*EndA). The residue at position 129 has identical conformation in the two enzymes, but Asn69 in *Vc*EndA folds such that it forms a hydrogen bond to the backbone N atom of residue 72, while Gln69 in Vvn extends out into the solvent region. Position 69 is at the periphery of the binding region defined by the Vvn–DNA complex and the longer Gln in Vvn form relatively short contacts to the sugar ring of the DNA backbone in the Vvn–DNA structure. The hydrogen bond between the Asn69 side chain and the main chain of Arg72 may lead to a stabilization of this loop region in *Vc*EndA. Other side chains in the DNA-binding region are of the same type, but are observed in different conformations in the two enzymes (*i.e.* 75, 95, 99 and 156). This could, however, just be a result of the large rotational space available in the uncomplexed structures.

4. Conclusion

In this paper, we report the structure of endonuclease I from *V. cholerae*. The structure was solved in a neutral-pH and a low-pH form. The structure of the endonuclease is essentially identical in the two forms, but the low-pH form displays the absence of a catalytically important magnesium ion. However, the conformation of the amino-acid residues and the solvent structure forming the magnesium-binding site is preserved in the two structures. The lack of magnesium may explain the strong reduction in activity of the enzyme beginning at pH 6.5 and proves the importance of the ion in the catalytic mechanism. Both structures also identify the presence of a chloride ion completely buried in the interior of the protein, about 7 Å from the nearest solvent molecule and about 10 Å from the position of the magnesium ion. The presence of such a completely buried chloride has to our knowledge only been reported for the hormone-binding domain of the atrial natriuretic peptide (ANP) receptor. The function of the chloride in *Vc*EndA is, however, not yet known.

The *Vc*EndA structure was compared with the homologous endonuclease from *V. vulnificus*. The catalytic domain of the two enzymes share 73% sequence identity and the fold is almost identical. Small differences exist in the orientation of side chains, but these are generally found in regions involved in crystal packing or in the DNA-binding region which is relatively open in the uncomplexed structures.

We thank Dr Solveig Karlsen for her help with the collection of the in-house X-ray diffraction data. The present study was supported by the National Functional Genomics Program (FUGE) of The Research Council of Norway and by Biotec-Pharmacon ASA. Provision of beamtime at the Swiss–Norwegian Beamlines (SNBL) at the European Synchrotron Radiation Facility (ESRF) is gratefully acknowledged.

References

Akker, F. van den, Zhang, X., Miyagi, M., Huo, X., Misono, K. S. & Yee, V. C. (2000). *Nature (London)*, **406**, 101–104.
Altermark, B. (2006). PhD thesis. University of Tromsø, Norway.
Collaborative Computational Project, Number 4 (1994). *Acta Cryst.* D**50**, 760–763.
DeLano, W. L. (2002). *The PyMOL Molecular Visualization System.* http://www.pymol.org.
Focareta, T. & Manning, P. A. (1987). *Gene*, **53**, 31–40.
Focareta, T. & Manning, P. A. (1991*a*). *Mol. Microbiol.* **5**, 2547–2555.
Focareta, T. & Manning, P. A. (1991*b*). *Gene*, **108**, 31–37.
Golovin, A., Dimitropoulos, D., Oldfield, T., Rachedi, A. & Henrick, K. (2005). *Proteins*, **58**, 190–199.
He, X.-L., Chow, D.-C., Martick, M. M. & Garcia, K. C. (2001). *Science*, **293**, 1657–1662.
Hooft, R. W., Vriend, G., Sander, C. & Abola, E. E. (1996). *Nature (London)*, **381**, 272.
Jones, T. A., Zou, J.-Y., Cowan, S. W. & Kjeldgaard, M. (1991). *Acta Cryst.* A**47**, 110–119.
Kraulis, P. J. (1991). *J. Appl. Cryst.* **24**, 946–950.
Laskowski, R. A., Moss, D. S. & Thornton, J. M. (1993). *J. Mol. Biol.* **231**, 1049–1067.
Li, C. L., Hor, L. I., Chang, Z. F., Tsai, L. C., Yang, W. Z. & Yuan, H. S. (2003). *EMBO J.* **22**, 4014–4025.
Murshudov, G. N., Vagin, A. A. & Dodson, E. J. (1997). *Acta Cryst.* D**53**, 240–255.
Ogawa, H., Qiu, Y., Ogata, C. M. & Misono, K. S. (2004). *J. Biol. Chem.* **279**, 28625–28631.
Perrakis, A., Morris, R. & Lamzin, V. S. (1999). *Nature Struct. Biol.* **6**, 458–463.
Powell, H. R. (1999). *Acta Cryst.* D**55**, 1690–1695.
Steiner, T. (1998). *Acta Cryst.* B**54**, 456–463.
Vagin, A. & Teplyakov, A. (1997). *J. Appl. Cryst.* **30**, 1022–1025.
Wu, S. I., Lo, S. K., Shao, C. P., Tsai, H. W. & Hor, L. I. (2001). *Appl. Environ. Microbiol.* **67**, 82–88.